

Rapid control prototyping development of vehicle semi-active control scheme

XiaoMin Dong *, Miao Yu, Changrong Liao, Weimin Chen

Center for Intelligent Structures Department of Optoelectronic Engineering, Chongqing University, 400044,
Chongqing, China

(Received December 2 2007, Accepted March 14 2008)

Abstract. This study discusses the rapid control prototyping approach used for development and investigation of control algorithm in magneto-rheological (MR) semi-active suspension system. Firstly, a multibody dynamic model based on MR suspension system is developed with the aid of VEDYNA software. Based on the model, a new intelligent control algorithm, human simulated intelligent control (HSIC) is proposed and designed. Finally, by means of dSPACE groupware system, the semi-active control prototype of real car has been built up, road test of real car and parameters of online adjustment have also been carried out. The results of offline simulation and real time control show that HSIC can achieve better comfort under assuring stability. They also show that rapid control prototyping (RCP) on the basis of Matlab/Simulink and dSPACE can shorten the research period of vehicle semi-active controller and reduce the cost of research. It is very significant to promote the industrialization of vehicle semi-active controller.

Keywords: rapid control prototyping (RCP), human-simulated intelligent control (HSIC), magneto-rheological, semi-active suspension

1 Introduction

Magneto-rheological fluids (MRF) change their viscosity depending on an externally applied magnetic field strength. The bandwidth of the resulting flow properties is large; the state varies between fluid and nearly solid material in a few milliseconds. Hence its flow, shear and squeeze process can be controlled using easily generated magnetic fields. MRF devices have additionally several advantageous control properties. MRF devices are continuously controllable and operate subject to almost no wear. In recent years, MR dampers have received much attention as semi-active system actuators for their rapid response to the applied magnetic field and their compact size.

A variety of control algorithms have been proposed for semi-active suspension. From skyhook, hybrid, LQG and fuzzy logic control schemes have been studied. Karnopp et al^[4] first proposed a skyhook control algorithm for a vehicle suspension system and demonstrated that this system can improve performance over a passive system when applied to a single-degree-of-freedom system. In [2] authors dealt with the effect of damping on the natural frequency of the tire, typically 10-12 Hz. With a passive damper, an increase in damping corresponds to higher body accelerations (less ride comfort), but less suspension deflection and more control of the wheel hop (better road handling). With the semi-active damper, however, an increase in damping showed improved ride, at the cost of increased wheel hop. To overcome the trade off between ride comfort and stability, a hybrid control algorithm is studied in [1]. The results show that the control algorithm offers benefits beyond those of conventional passive damping system. Dyke et al. applied a clipped-optimal control strategy (LQG) based on acceleration feedback. The performance of LQG or LQR controllers is dependent upon the choice of weighting matrices for the vector of regulated responses and control forces. When the cost function weighting matrices are changed, the response of the system can be greatly changed and the values

* Corresponding author. E-mail address: xmdong@cqu.edu.cn.

in the weighting matrices are often determined by trial and error. Kim and Lee (2003) applied Lyapunov's direct approach to a multi-degrees of-freedom suspension system. Lai and Liao developed a sliding mode controller theory for a suspension system with an MR damper. More recently some control strategies based on intelligent control theory have also been proposed for MR damper^[5, 6, 9]. Fang and Chen^[5] applied a fuzzy control strategy to a 4-DOF vehicle model and developed a useful control strategy.

Several semi-active control methods have been identified in the prior art. Most of these studies have focused only on numerical simulation studies, without any experimental confirmation, or without analytical treatment of nonlinear system equations. The reasons may possibly be attributed to the complexity of the controlled object. It is difficult to build an accurate dynamic model of MR suspension for its significant non-linearity, uncertainty and time-delay. Experimental confirmation also means expensive and time-consuming.

Recently, the computer aided control system design (CACSD) has been the subject of focus. The CACSD is often named as the rapid control prototyping (RCP) or the hardware-in-the-loop simulations (HILS). In the RCP, the plant dynamics and/or the controller are implemented in a digital signal processing board, which allows an easy adjustment of various parameters of the plant and/or the controller. If actual hard-wares are used in simulating the dynamic performance of a controller and/or a plant model, the word "HILS" is particularly used. Through the CACSD, the total development time and cost can be much reduced. Also it is to introduce a new component or a new algorithm because the test procedure, once it is set up, can be easily repeated.

In this paper, a new intelligent control algorithm, human simulated intelligent control (HSIC), for the MR suspension system and the CACSD through the RCP and HILS are investigated. First, a full car nonlinear multi-body dynamic model of MR suspension system is built based on VEDYNA software. Then HSIC controller is designed and numerical simulation is carried out. At last, with the aid of dSPACE, road test of MR suspension system is also carried out.

2 Modelling of full car multibody dynamics

Due to nonlinearity, uncertainty and time-delay, it is difficult to build an accurate dynamic model for MR suspension system. Depending upon the specific design purpose for the dynamical model, a reduction of the system dimension can often be achieved. In this study, a saloon car is selected as research object. The virtual car model of the saloon car is built with the aid of VEDYNA multi-body dynamic software. The vehicle model of VEDYNA^[3] consists of a system of nine rigid bodies comprising the vehicle body, the axle suspensions and the wheels in Fig. 1. Further sub-models are employed to depict the characteristics of the drive train, the steering mechanism, and the tires. Suitable minimum coordinates and generalized velocities are used to describe the spatial state of the vehicle and its components. The equations of motion that are derived from Jourdain's Principle can be written^[3]:

$$M_{BV}(y_{BV}) = Q_{BV}(y_{BV}, z_{BV}, y_{ST}, z_{ST}, y_{DT}, z_{DT}) \quad (1)$$

$$\dot{y} = K_{BV}^{-1}(y_{BV})z_{BV} \quad (2)$$

$$M_{DT}z_{DT} = Q_{DT}(y_{DT}, z_{DT}) \quad (3)$$

$$y_{DT} = V_{DT}z_{DT} \quad (4)$$

$$M_{ST}(y_{ST}, y_{BV})y_{ST} = Q_{ST}(y_{ST}, z_{ST}) \quad (5)$$

$$y_{ST} = V_{ST}z_{ST} \quad (6)$$

$$Dy_T = F_{stat} - Cy_t \quad (7)$$

Where, equations (1) and (2) characterize the vehicle dynamics comprising the vehicle body and axles by the 24 first-order ordinary differential equations (ODEs). Eight ODEs (7) describe the lateral and longitudinal deviations of the tires by means of spring and damper elements. The dynamic model of the drive train consists of 19 ODEs, (3) and (4), including four equations governing the angular wheel speeds. Five additional ODEs account for the dynamics of the steering system (5) and (6).

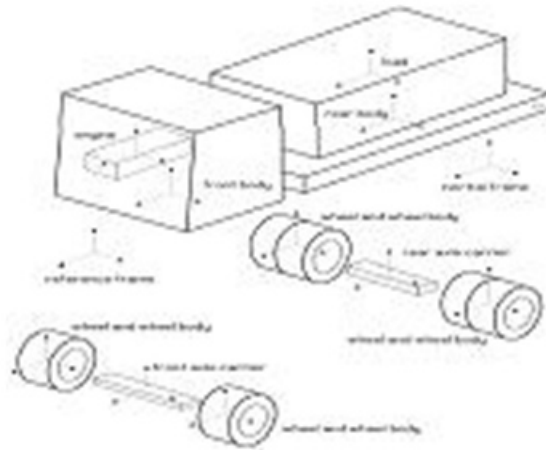


Fig. 1. Full vehicle dynamics model of VEDYNA

In order to simulate MR suspension system, those damper elements in equation (7) is replaced by MR damper. The control damping force u of MR damper is composed of velocity damping force and Coulomb friction^[10].

$$u = -C_e V + F_{MR} \tag{8}$$

where C_e is damping coefficient, F_{MR} is controllable damping force and V is velocity of piston.

3 Off line design of controller and simulation

3.1 Off line design of HSIC controller

A HSIC controller consists of three levels^[7]. As the lowest level of HSIC, direct control level, based on the characteristic mode of a car, one corresponding control means is selected to directly control MR dampers among bang-bang control, holding mode control and proportional plus differential control. As the second level, parameter correction level, adjusts the parameters of the direct control level. As the third level, task adjustment level, deals with the linearization and the time-delay compensation.

3.1.1 Direct control level

The real line trace in Fig. 2 is the ideal target trajectory $f_d(e, \dot{e})$. Where e represents the heave velocity of car body, \dot{e} denotes the heave acceleration of car body. We have taken the following methods to make the actual error trajectory keep as close with the ideal error trajectory.

Characteristic elements set:

$$Q_1 = \{q_{11}, q_{12}, q_{13}, q_{14}, q_{15}\} \tag{9}$$

in which $q_{11} \Rightarrow |e| < \delta_1, q_{12} \Rightarrow |e| < \delta_2, q_{13} \Rightarrow e\dot{e} > 0, q_{14} \Rightarrow |\dot{e}/e| < c_1, q_{15} \Rightarrow |\dot{e}/e| < c_2$ and c_1, c_2 are the slopes of line S_1 and S_2 .

Characteristic model can be written by

$$\Phi_1 = \{\phi_{11}, \phi_{12}, \phi_{13}, \phi_{14}, \phi_{15}\} \tag{10}$$

where $\phi_{11} = (q_{11} \cup q_{12}) \cap q_{13}, \phi_{12} = (q_{11} \cup q_{12}) \cap q_{13} \cap q_{14}, \phi_{13} = (q_{11} \cup q_{12}) \cap q_{14} \cap q_{15}, \phi_{14} = (q_{11} \cup q_{12}) \cap q_{13} \cap q_{15}$.

The control mode set of the direct control level is shown as:

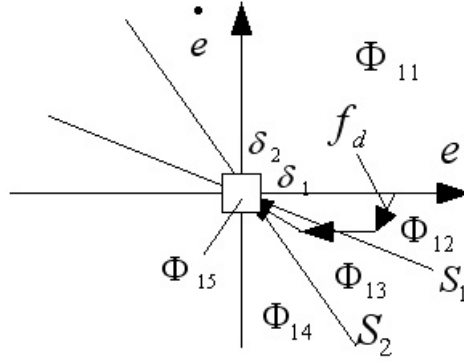


Fig. 2. Characteristic model of direct control level

$$\Psi_1 = \{\psi_{11}, \psi_{12}, \psi_{13}, \psi_{14}, \psi_{15}\} \quad (11)$$

Where $\psi_{11} = K_p e + kK_p \sum_{i=1}^n e_{m,i}$, $\psi_{12} = (1 - k)K_p e + kK_p \sum_{i=1}^n e_{m,i}$, $\psi_{13} = kK_p \sum_{i=1}^n e_{m,i}$, $\psi_{14} = -K'_p e + kK_p \sum_{i=1}^n e_{m,i}$, $\psi_{15} = kK_p \sum_{i=1}^n e_{m,i} + K_I \int e(t) dt$.

in which K_p, k, k'_p, K_I represent proportional coefficient, modified coefficient, modified proportional coefficient and integral coefficient respectively.

The reference rule set of the direct control level is shown as:

$$\Omega_1 = \{\omega_{11}, \omega_{12}, \omega_{13}, \omega_{14}, \omega_{15}\} \quad (12)$$

where $\omega_{11} \Rightarrow \phi_{11} \rightarrow \psi_{11}$, $\omega_{12} \Rightarrow \phi_{12} \rightarrow \psi_{12}$, $\omega_{13} \Rightarrow \phi_{13} \rightarrow \psi_{13}$, $\omega_{14} \Rightarrow \phi_{14} \rightarrow \psi_{14}$, $\omega_{15} \Rightarrow \phi_{15} \rightarrow \psi_{15}$.

3.1.2 Parameter correction level

At parameter correction level, some characteristic elements set is

$$Q_2 = \{q_{21}, q_{22}, q_{23}, q_{24}, q_{25}, q_{26}\} \quad (13)$$

in which $q_{21} \Rightarrow |e|\delta_1$, $q_{22} \Rightarrow |e|\delta_2$, $q_{23} \Rightarrow |e_{m,j}| > \alpha$, $q_{24} \Rightarrow |e_{m,j-1}| > \alpha$, $q_{25} \Rightarrow \Delta e \cdot e \geq 0$, $q_{26} \Rightarrow \Delta \dot{e} \cdot \dot{e} \geq 0$.

Characteristic model can be written as:

$$\Phi_2 = \{\phi_{21}, \phi_{22}, \phi_{23}, \phi_{24}, \phi_{25}\} \quad (14)$$

where $\phi_{21} = q_{21} \cap q_{22} \cap q_{23} \cap q_{24}$, $\phi_{22} = q_{21} \cap q_{22} \cap q_{23} \cap q_{24}$, $\phi_{23} = q_{21} \cap q_{22} \cap q_{25}$, $\phi_{24} = (q_{21} \cap q_{22} \cap q_{25} \cap q_{26})$, $\phi_{25} = (q_{21} \cap q_{22} \cap q_{25} \cap q_{26})$.

The reference rule set of the direct control level is shown as:

$$\Omega_2 = \{\omega_{21}, \omega_{22}, \omega_{23}, \omega_{24}, \omega_{25}\} \quad (15)$$

where $\omega_{21} \Rightarrow \phi_{21} \rightarrow \psi_{21}$, $\omega_{22} \Rightarrow \phi_{22} \rightarrow \psi_{22}$, $\omega_{23} \Rightarrow \phi_{23} \rightarrow \psi_{23}$, $\omega_{24} \Rightarrow \phi_{24} \rightarrow \psi_{24}$, $\omega_{25} \Rightarrow \phi_{25} \rightarrow \psi_{25}$.

Parameter correction model set:

$$\Psi_2 = \{\psi_{21}, \psi_{22}, \psi_{23}, \psi_{24}\} \quad (16)$$

Where $\psi_{21} \Rightarrow K_p = (1 + w_1 e_{m,i} / e_{m,i-1}) K_p$, $\psi_{22} \Rightarrow K'_p = (1 - w_1 e_{m,i} / e_{m,i-1}) K'_p$, $\psi_{23} \Rightarrow K_I = w_2$, $\psi_{24} \Rightarrow K_I = -w_2$, $\psi_{25} \Rightarrow K_I = 0$.

in which w_1 and w_2 denote positive modified coefficients $e_{m,i}$ and $e_{m,i-1}$ represent i th and $i - 1$ th error peak values.

3.1.3 Task adjustment level

Generally speaking, there is not a corresponding characteristic model to indicate a task adjustment. In this paper, task adjustment level deals with the linearization for nonlinear MR damper and the compensation for time-delay. Therefore, it is important to know the actual time-delay magnitude for achieving good control performance. To achieve this, an experimental apparatus was founded to measure the time-delay. The MR damper was actuated by a Material Test System (MTS) load frame. A triangle wave input signal had to be chosen that would ensure constant velocity across the damper. An acceleration peak $a(t)$ will appear while the direction of damper pole is changed. This peak signal could be transformed into passive pulse $v_0(t)$ by Schmitt trigger. The pulse signal was used to trigger a signal generator to output a continuous square wave $V_c(t)$ applied to current driver as step control signal. So the current driver would output various current from 0.2 Amps to 1.6 Amps to adjust damping force $F(t)$ of MR damper. The response time of MR suspension was defined as the time required to make the transition from control signal applied to 63.2% of the final state of damping force, or one time constant. The measured results that the response time is not affected by the applied current, but it can be considered as a function of piston velocity V (shown in Tab. 1 and Tab. 2).

$$\tau = 38.0V + 15.0333 \quad (17)$$

Table 1. MR dampers' response time via applied current at 0.1m/s

τ (ms)	V(m/s)	0.1	0.2	0.3
Response		15.5	23.3	26.1

Table 2. MR dampers' response time vs. piston velocity

τ (ms)	I(A)	0.8	1.0	1.2	1.4	1.6
Response		14.1	14.3	14.9	14.8	16.6

According to above analysis, the time-delay of MR damper is about 25 ms, which will degrade the performance of semi-active control. Therefore, it is necessary to compensate the time-delay in the design of HSIC controller. Time-delay compensation by using Smith's predictor.

In this paper, the linear function is defined as $s = c\dot{x}$, where s is the set force value, \dot{x} is the damper velocity, c is the set point gain, and control signal is current. Therefore, to induce the MR damper to generate approximately the corresponding desired control forces F_{dfl} , F_{dfr} , F_{drl} and F_{drr} , the command signal current is selected as follows. The damping force of MR damper is fed back with a feedback gain B and compared to the desired force. The resulting error is scaled using a proportional gain G . MR damper cannot add energy to the system. As a result, only when the direction of damping force and the error are the same direction, the HSIC controller can operate. If they have different sign, the command input current of MR is set to be zero. The corrected control signal is then saturated between the maximum and minimum current.

3.1.4 The parameters of hsic are determined by HTGA

Some threshold parameters of HSIC that need to be determined initially are δ_1 , δ_2 , c_1 , c_2 , k , α , w_1 and w_2 , the others such as K_p , K'_p and K_I can be adjusted at parameter correction level while running. The course of determination for those threshold value parameters needs much trial or error. Therefore, in this paper, a HTGA^[8] is proposed to tune the parameters.

Encoding

The real number encoding is adopted in this paper. The length of chromosome is determined by the number of the threshold parameters. Fitness function

To choose the ideal threshold value parameters, a tradeoff is assumed between ride comfort and stability. Therefore, the fitness function is chosen as:

$$Fit = a \sqrt{\frac{1}{T} \int_0^T \ddot{x}_s^2 dt} + (1 - a) \sqrt{\frac{1}{T} \int_0^T \ddot{x}_u^2 dt} \quad (18)$$

Where a represents the weighting factor, T is simulation time. \ddot{x}_s and \ddot{x}_u are accelerations of sprung mass and unsprung mass of monocorner suspension respectively.

Crossover and mutation

The crossover operators used here are one-cut-point crossover by convex crossover. After generation of diverse offspring by crossover operation, the orthogonal arrays of Taguchi method are used to study the 8 parameters of HSIC controller with a small number of experiments. In this work, a two level orthogonal array $L_{16}(2^{15})$ is used. The $L_{16}(2^{15})$ represents 15 columns and 16 individual experiments corresponding to 16 rows, only the first 8 columns are used, and the other 7 columns are ignored. The best level for each gene is determined from two chromosome chosen randomly at each run by orthogonal experiments with 16 times. Once the optimal level of each gene is selected, one can obtain the optimal chromosomes. The mutation operator used in this paper is convex combination.

3.2 Simulation

VEDYNA provides a graphic simulation environment by a combination of C-code and Simulink. The HSIC control is implemented by use of the S-functions in the Simulink in fig. 3. In fig.4, the Input States block is the standard block of VEDYNA which is read from workspace, the control modal select block executes the association function of HSIC controller, SIMC1-SIMC9 are nine control modal, and the write to workspace block implements output of control damping force transferred by vehicle dynamic model. The effect of

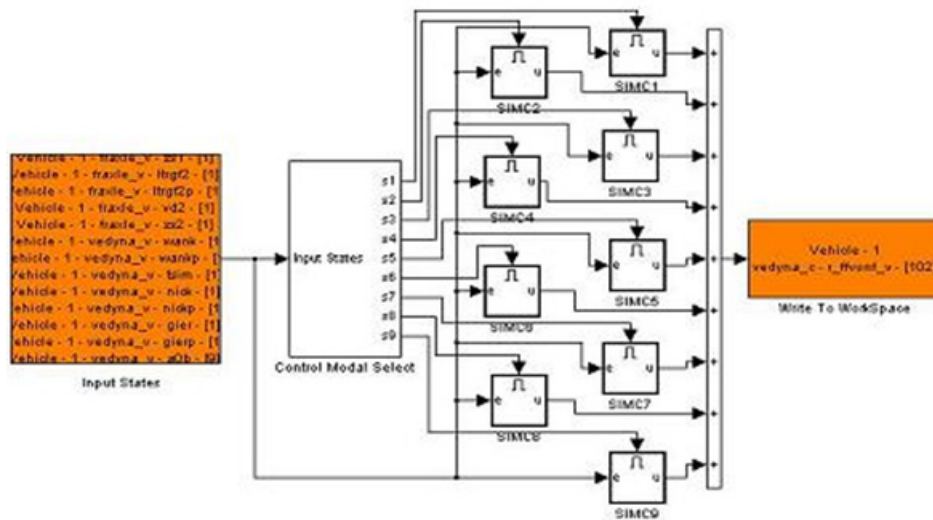


Fig. 3. Block diagram of simulation for HSIC controller

different MR damping force on ride comfort and stability is investigated by numerical simulation. Random road are selected. The vehicle velocity is 40 kilometer per hour. The results are show in Fig. 4 and 5. From the two figures, we can see that semi-active suspension with HSIC can depress heave vibration compared to passive suspension.

4 Road test

To verify the actual control performance, the control system based on dSPACE that consists of DS1005 PPC board, DS2002 multi-Channel A/D Board and DS2102 high-resolution D/A Board, is fabricated. The

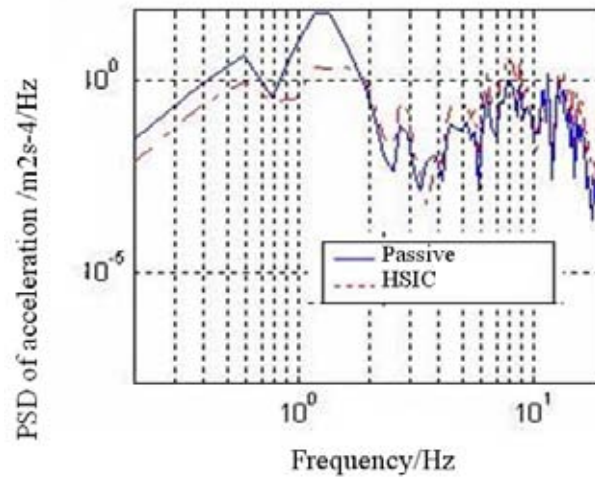


Fig. 4. PSD of heave acceleration at 40km/h

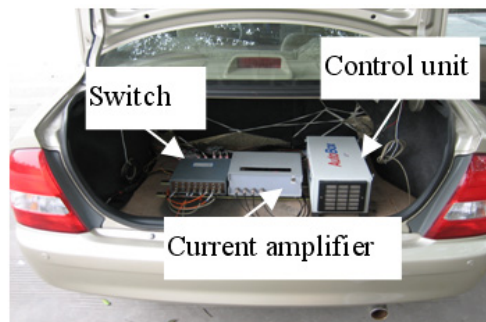


Fig. 5. Location of the electronic hardware in the test vehicle

control algorithm is implemented on a rapid prototyping unit, the dSPACE AutoBox in Fig. 5. The electronic hardware consists of a current amplifier, a switch and the electronic control unit. Mazda 323 is selected as experimental car. Four MR shock absorbers are used to replace the passive ones. Four accelerometers are placed on carriage's foursquare floor to record the vertical accelerate signal of sprung mass. Other four accelerometers are placed on two axis of vehicle to record the vertical accelerate signal of unsprung mass. Every seat has a passenger to simulate the condition of full load. The road test is carried out on gravel road with class D surface at 30Km/h. The results is shown in Fig. 6 which clearly present that the vibration of vehicle body between 4 and 12.5 Hz is significantly reduced, but the semi-active suspension system has minimal effect on suppressing higher mode vibration.

5 Conclusion

In this study, the control design and implementation for MR suspension is largely supported by VEDYNA and rapid control prototyping system. The performances of the suspension system under random road excitations are evaluated through computer simulation. Under random excitation, the ability of MR dampers by the control of HSIC controller to reduce RMS amplitudes is also shown, which means that HSIC can achieve better ride comfort than passive suspension. To verify the actual control performance, road test based on dSPACE is also carried out on class D road surface. The experimental results show that the semi-active suspension based on HSIC controller can achieve better comfort than the passive. They also show that rapid control prototyping (RCP) for MR suspension system can shorten the research period of vehicle semi-active controller and reduce the cost of research.

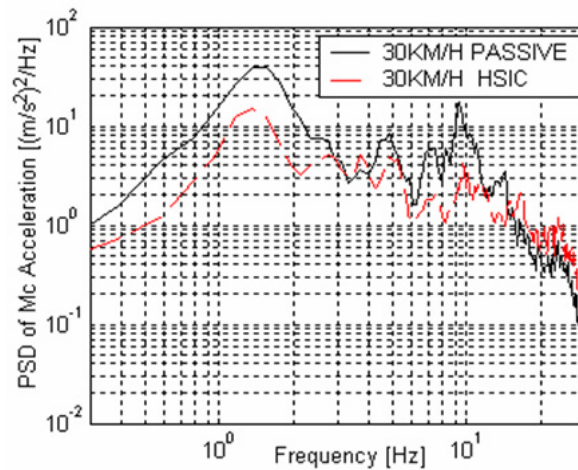


Fig. 6. Acceleration Power Spectrum density of sprung Mass (30Km/h, class D of road profile)

References

- [1] M. Ahmadian. A hybrid semiactive control for secondary suspension applications. **in:** *Proceedings of the Sixth ASME Symposium on Advanced Automotive Technologies*, 1997 ASME International Congress and Exposition, 1997.
- [2] M. Ahmadian, R. H. Marjoram. Effects of passive and semiactive suspensions on body and wheel hop control. *Journal of Commercial Vehicles*, 1989, **98**: 596–604.
- [3] C. Chucholowski, M. V. ogel, O. von Stryk, T. M. Wolter. Real time simulation and online control for virtual test drives of cars. *High Performance Scientific and Engineering Computing*. Lecture Notes in Co.
- [4] M. J. Crosby, R. A. Harwood, D. Karnopp. Vibration control using semi-active force generators. *Lord Library of Technical Articles*, 1973.
- [5] X. Fang, W. Chen, L. Wu, Q. Wang, et al. Fuzzy control technology and the application to vehicle semi-active suspension. *Chinese Journal of Mechanical Engineering*, 1999, **35**(3): 98–100.
- [6] A. H.-F. Lam, W.-H. Liao. Semi-active control of automotive suspension systems with magneto-rheological dampers. *International Journal of Vehicle Design*, 2003, **33**: 50–75.
- [7] Z. Li. A study on intelligent control theory. *Information and Control*, 1991, **20**(5): 27–38.
- [8] J.-T. Tsai, T.-K. Liu, J.-H. Chou. Hybrid taguchi-genetic algorithm for global numerical optimization. *IEEE Transaction on evolutionary computer*, 2004, **8**(4): 365–377.
- [9] M. Yokoyama, J. K. Hedrick, S. Toyama. A model following sliding mode controller for semi-active suspension systems with mr dampers. **in:** *Proceedings of the American Control Conference Arlington*, 2001, 2652–2657.
- [10] M. Yu, C. R. Liao, W. Chen, S. L. Huang. Study on mr semi-active suspension system and its road testing. **in:** *Proceedings of International Symposium on Smart Materials for Engineering and Biomedical Applications, SMEBA 2004, China*, 2004, 349–353.